A metaplate for complete 3D vibration isolation

Zhichao Yao[a], Ruixue Zhao[b] , Valentina Zega[b] and Alberto Corigliano[b,*]

[a] *School of Mechanical Engineering, Nanjing University of Science and Technology, Nanjing 210094, People's Republic of China*
[b] *Department of Civil and Environmental Engineering, Politecnico di Milano, Milano 20133, Italy*

E-mail: alberto.corigliano@polimi.it

Abstract

This paper presents a new metamaterial plate (metaplate) made by a periodic repetition of 'frame-springs-mass' systems for vibration isolation. Numerical studies and experimental measurements demonstrate that the proposed structure show a complete 3D phononic bandgap in the low-frequency range. In the numerical computation of the transmission diagram, the self-weight gravity, the material damping, the geometry of the metaplate and different boundary conditions are considered. A prototype of the proposed metaplate, made of Polyamide, is fabricated by means of additive manufacturing and experimentally tested. The measured transmission diagram is in good agreement with numerical predictions, thus proving the proposed design and promoting potential applications such as low-frequency vibration isolation and stress wave mitigation.

Keywords: metaplate, periodic structure, complete bandgap, vibration isolation

1. Introduction

In recent years, the propagation of elastic waves in artificial structures has attracted a lot of interest expecially for the study of emergent properties such as the opening of bandgaps (i.e. frequency ranges where the propagation of elastic/acoustic waves is prohibited). The existence of this property, in fact, opens the way to several interesting applications such as vibration isolation (Chen et al., 2016; D'Alessandro et al., 2016; D'Alessandro et al., 2017a) and noise reduction (Mei et al., 2012; Xiao et al., 2012).

Periodic structures exhibiting bandgaps can generally be divided into two main categories: (1) phononic crystals and (2) locally resonant metamaterials (Bilal et al., 2017).

Phononic crystals(PC) are material systems with spatially periodic distributed unit cells that exhibit bandgaps by exploiting the Bragg scattering. For this reason, they can attenuate waves with the wavelength of the same order of their periodic unit cell sizes (Kushuwaha, 1993).

Locally resonant metamaterials are instead periodic or non-periodic artificial materials with unit cells possessing resonating elements. The mechanism producing bandgaps is based on local resonance and for this reason, they can attenuate waves with the wavelength of two orders of magnitude larger than their unit cell size (Liu et al., 2000).

Among this large variety of artificial materials exhibiting bandgaps, elastic metaplates are of great importance thanks to their potential engineering applications. They can be classified into two types based on the location of the periodic inclusions: (1) flat elastic metaplates and (2) stubbed elastic metaplates (Khelif and Adibi, 2015).

In the flat elastic metaplate, periodic array of inclusions are embedded inside a homogeneous plate. These inclusions can be either filled with another material, be void, or partially filled and partially void. As some meaningful examples, Yu *et al* studied the bandgap property of a plastic thin plate with Pb block coating the soft rubber periodic inclusions (Dian-Long et al., 2005). Charles *et al* demonstrated that inclusions heavier and stiffer than the background material are required to allow the opening of bandgaps (Reinke et al., 2011). Zhu *et al* proposed a thin plate with periodic cantilever-mass microstructures for low-frequency bandgap applications (Zhu et al., 2011). To the authors knowledge, a lot of works focus on the study of the bandgap properties of flat elastic metaplates (Chen et al., 2012; Olsson et al., 2008; Ardito et al., 2016), but no low-frequency complete bandgaps have been found so far in such kind of materials.

On the other side, stubbed elastic metaplates that consist in arrays of stubs on top of solid slabs were first demonstrated by Wu *et al*. They demonstrated that the complete bandgap is found when the stub height reaches about three times the plate thickness (Wu et al., 2008). Based on their work, Bilal *et al* (Bilal and Hussein, 2013) investigated the bandgap characteristics of a metaplate with arrays of both holes and stubs and they found that it is possible to broaden the bandgaps by exploiting the trampoline effect. Assouar *et al* then studied the bandgap of a double-side stubbed metaplate (Badreddine Assouar and

Oudich, 2012) and demonstrated that the relative bandwidth increases by a factor of 2 compared to the classical one-side stubbed plates. Zhao *et al* investigated the flexural vibration bandgaps of the double-side stubbed metaplate proposed in (Zhao et al., 2015) and found that a significant enlargement of the bandwidth of flexural vibration bandgaps can be obtained. Later, they proposed a double-vibrator (rubber–steel–rubber–steel layers) three-component pillared PC plate that can also show the opening of a bandgap (Zhao et al., 2016). Recently, Li *et al* designed a new structure which consists of periodic double-sided novel composite resonators, deposited on a 2D locally-resonant phononic-crystals plate made of a rubber-filler array, which is embedded in an epoxy plate (Li et al., 2019). They showed that in such a way it is possible to achieve a significant increase in the absolute bandwidth (i.e. by a factor of 4.2) with respect of the conventional phononic crystals. The stubbed elastic metaplates, however, may have limits for some specific engineering applications due to the requirement of increased weight and thickness of the plate.

Finally, both flat and stubbed elastic metaplates usually require the combination of two or more materials to exploit the opening of the bandgap (Li et al., 2019, 2017; Zhao et al., 2015, 2016) and this makes the fabrication and assembly procedure complex and expensive. For engineering applications such as the one we are focusing in this paper (i.e. vibration isolation), a metaplate made by a single material and easily fabricable through additive manufactoring is auspicable (D'Alessandro et al., 2016; D'Alessandro et al., 2017b).

We then propose an elastic metaplate for vibration isolation and we prove that a full 3D bandgap can be achieved through a proper design of its mechanical structure.

In Section 2, the mechanical design of the metaplate is presented, while the computation of the 3D bandgap through the finite element software COMSOLMultiphysics is reported in Section 3. The transmission analysis numerically computed, is then reported in Section 4 for different damping properties of the material, geometries of the metaplate and different boundary conditions. The effect of the gravity in the transmissibility property is also investigated in the same section. In Section 5, the prototype fabricated by means of additive manufacturing is experimentally tested and the measurements are compared with the numerical findings. Conclusions are finally reported in Section 6.

2. Metaplate for vibration isolation

The metaplate studied in this work is made by a periodic repetition of a unit-cell that consists of a square block connected to the external frame through folded beams properly designed to achieve a full 3D bandgap at low frequency (see close-up view in Fig. 1a). Four anchor points and a central area are also added to test the vibration isolation property of the proposed metaplate (see Fig. 1a). The idea is to apply external vibrations on the anchor points and measure the response at the central area: a complete isolation is expected within the bandgap of the metaplate. The proposed metaplate has overall dimensions of 0.28m × 0.28 m × 0.15 m and is fabricated in Polyamide PA2200 (Young's modulus E = 1.65 GPa, Poisson's ratio ν = 0.4, density ρ = 930 kg/m^3) through 3D-printing (see Fig. 1b) (Prosilas).

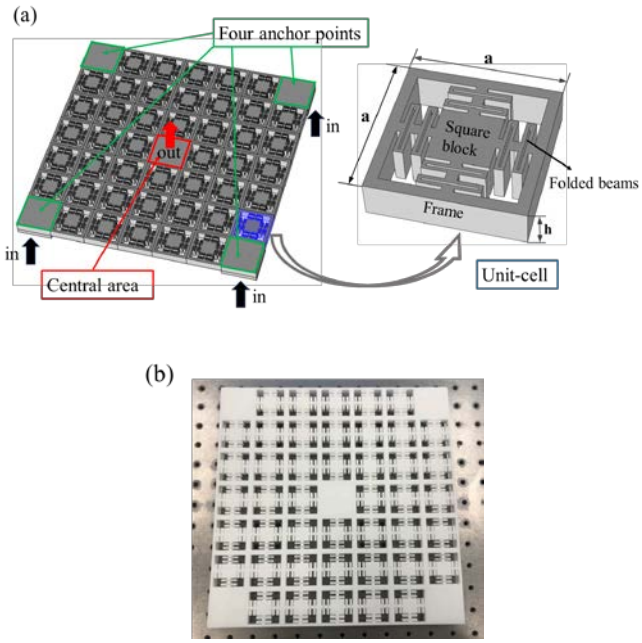

Fig. 1. (a) Schematic view of the proposed metaplate and close-up view of the unit-cell. (b) 3D-printed prototype.

3. Unit-cell design and bandgap analysis

Fig. 2a shows the in-plane schematic view of the unit cell of the metaplate here proposed. The main geometric parameters reported in Table 1 are defined as follows: the lattice constant and the plate thickness are denoted by a and h, respectively, while the length and other geometrical parameters of the folded beams are denoted by $L1$, $L2$, $L3$, and $L4$(Fig. 2a).

According to the heuristic model proposed in (Hirsekorn, 2004), the unit cell of Fig. 2a can be schematized as a 'frame-spring-mass' system, where the square block represents the 'mass' and the folded beams represent the 'springs'. Note that springs are properly designed to allow the movement of the mass along the three orthogonal directions thus guaranteeing a full 3D bandgap as it will be shown in the following.

To investigate the elastic wave attenuation and vibration isolation property of the proposed metaplate, the phononic

band structure is numerically computed by applying the Bloch theorem (D'Alessandro et al., 2016; D'Alessandro et al., 2017b; Ardito et al., 2018). Stress-free boundary conditions are applied on the free surfaces along the *z*-direction, while periodic conditions are applied at the boundaries between the unit cell and its two adjacent cells along the two in-plane directions. The Bloch theorem then reads (Oudich et al., 2010):

$$u_j(x+a, y+a) = u_j(x, y)e^{i(k_x a + k_y a)}, \quad (j = x, y, z) \tag{1}$$

where u_j denotes the elastic displacement vector along the *x*-, *y*-, and *z*- directions and k_x and k_y are the components of the Bloch wave vector. Thanks to the periodicity along both *x*- and *y*- directions and the symmetry of the unit cell, it is possible to evaluate the Bloch wave vector only along the border of the irreducible Brillouin Zone (Khelif and Adibi, 2015; Hedayatrasa, 2018). By varying the value of Bloch wave vector along the boundaries of the irreducible first Brillouin zone (as shown in Fig. 2b) and solving the eigenvalue problem generated by the finite element method, we can obtain the band structures (i.e. dispersion relations) for the proposed metaplate. The commercial software COMSOL Multiphysics version 5.4 is adopted to implement the FEM calculation procedures. The meshed unit cell with applied periodic boundary is shown in Fig. 2c for the sake of clarity.

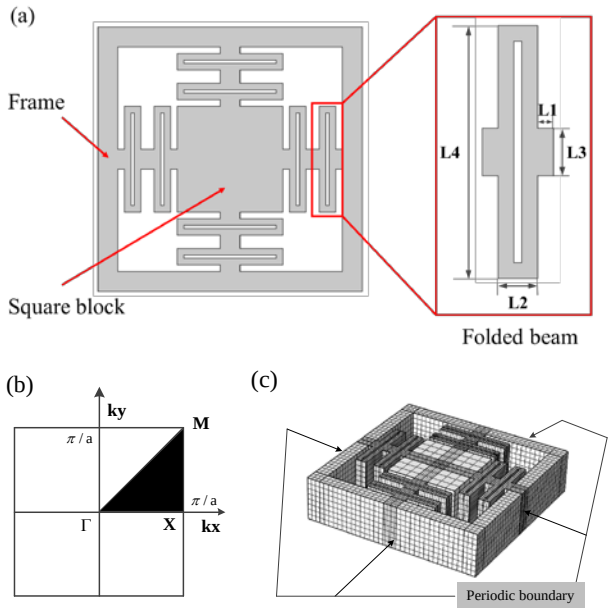

Fig. 2. (a) Unit cell of the proposed structure. (b) The first Brillouin zone. (c) Meshed unit-cell with applied periodic boundary conditions in COMSOLMultiphysics.

In Fig. 3 the dispersion relations computed for an infinite metaplate is shown: a complete 3D bandgap (red region) can be found from 1094Hz to 1436Hz between the third and fourth branches.

Table 1. Structure parameters

Parameters	Value	Parameters	Value
a	40 mm	*L2*	2.5 mm
h	10 mm	*L3*	3 mm
L1	1 mm	*L4*	16 mm

The opening and closing modes of the bandgap are labeled as mode A and mode B in Fig. 3a. Their shape functions are shown in Fig. 3b and 3c, respectively: mode A is the translational motion of the mass in the *x*- direction, while mode B is the translational motion of the mass and partially of the frame along the *z*-axis.

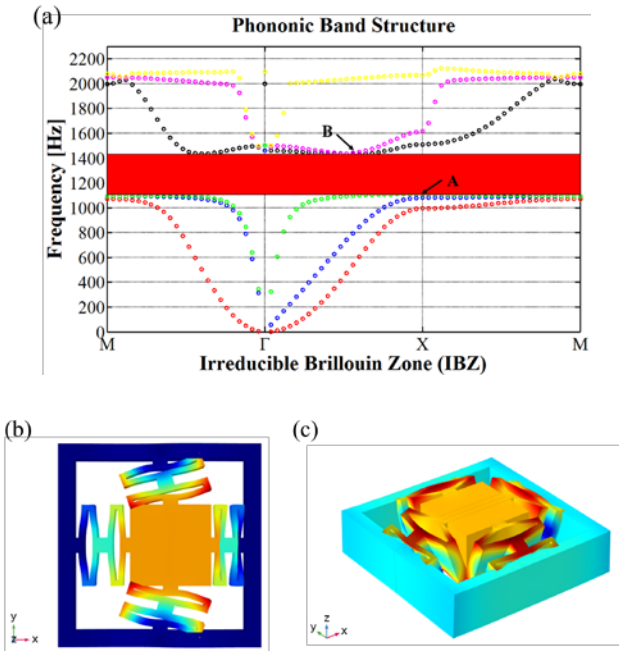

Fig. 3. (a) Dispersion diagram of the unit cell shown in Fig. 2a. (b) Mode A of the unit cell at *f*=1094Hz. (c) Mode B of the unit cell at *f*=1436Hz. The contour of the displacement field is shown in color.

4. Transmission spectrum analysis of the metaplate

To verify the existence of the bandgaps in the real prototype made by a finite number of unit-cells along the two in-plane directions, the transmission analysis is numerically obtained. Firstly, a purely linear elastic behavior of the Polyamide is considered thus neglecting every source of material damping. A displacement excitation d_{in} is imposed on the four anchor points along the two directions *x*- and *z*- and the average displacement response d_{out} along the two directions is measured on the middle of the plate (refer to Fig. 1a). Note that due to the in-plane (*xy*) symmetry of the metaplate here we report only the transmission analysis along the *x*- and *z*- directions: along the *y*- direction we expect the same results computed along the *x*- axis. The transmission T_d is defined as

$$T_d = 20\log\frac{|d_{out}|}{|d_{in}|}. \quad (2)$$

The transmission diagrams numerically computed along the *x*- (or *y-)* and *z*- directions are shown in Figs. 4a and b, respectively (the gray shadow region denotes the band gap of Fig. 3a). As a comparison, the transmission diagrams computed for an homogeneous solid plate of the same size of the metaplate under study are also shown in Figs. 4a and b in red dashed lines. From Fig. 4, it is evident that a sharp attenuation takes place inside the bandgap and that the attenuation level along the *x*- (or *y-)* and *z*- directions is very similar. In addition, we can notice that there are three local modes in the frequency range of the bandgap and the relative modal shape functions are shown in Figs. 4c-e, respectively.

4.1. The effect of self-weight gravity

In practical vibration isolation applications, the effects of self-weight gravity are not negligible (Dankowski, 1999; Ramsey and Wierschem, 2017). The metaplate can in fact deform under the effect of its self-weight and its bandgap's property can change accordingly.

To study the effect of the self-weight on the metaplate response, the gravity is added in the FEM model as a body load and the four anchor points are fixed to mimic the testing conditions(see Fig. 1a). A static analysis is then performed in COMSOLMultiphysics and the maximum displacement in the *z*-direction is found to be 34.4 μm. Fig. 5 shows the displacement component along the *z*-direction resulting from the application of the gravity on the metaplate. Note that the deformed shape is amplified by a factor of 300 for the sake of clarity. We then computed the transmission diagram by taking into account the effect of the gravity on the structure see Fig. 6. The introduction of the self-weight gravity results in a very small change of the transmission diagram. This result can be justified by the fact that the material of the prototype has a low mass density.

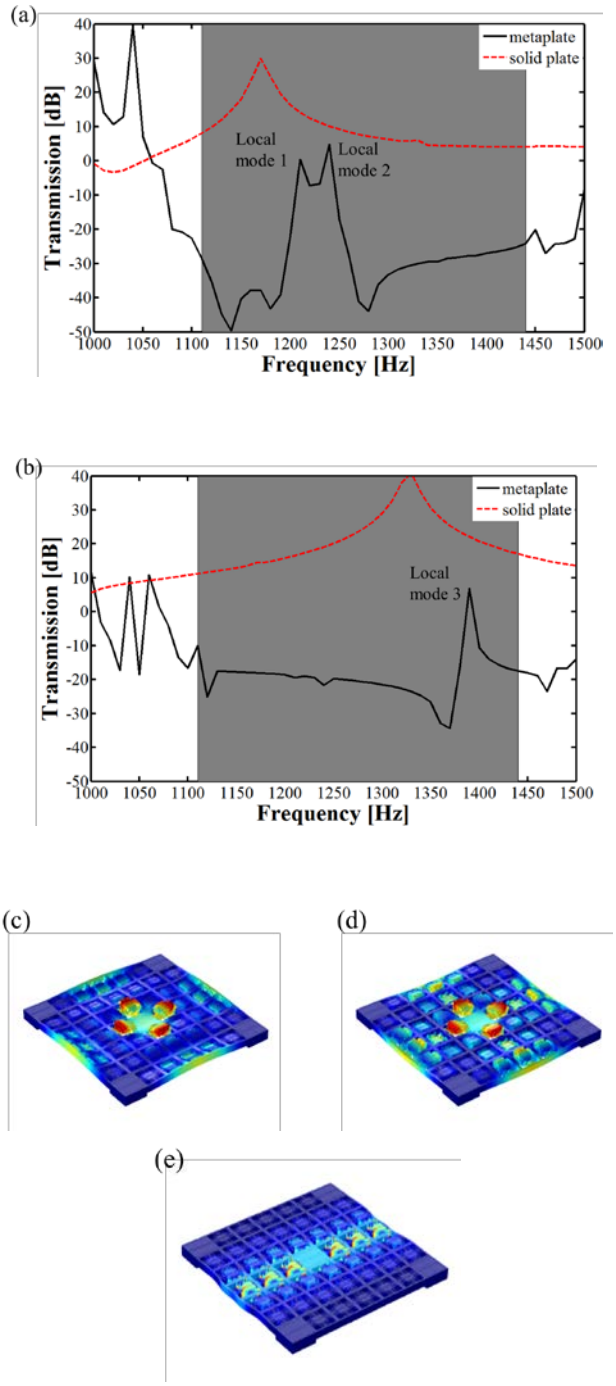

Fig. 4. (a) Transmission diagram along the (a) *x*- (or *y*-) and (b) *z*-directions. (c)-(e) Modal shape functions of local mode 1-3. The contour of the displacement field is shown in color.

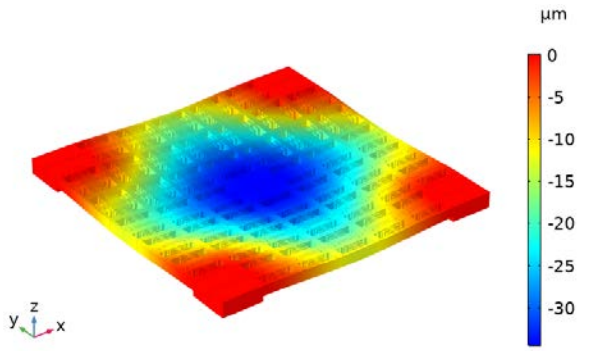

Fig. 5. *z*- displacement of the metaplate computed as a result of the effect of gravity.

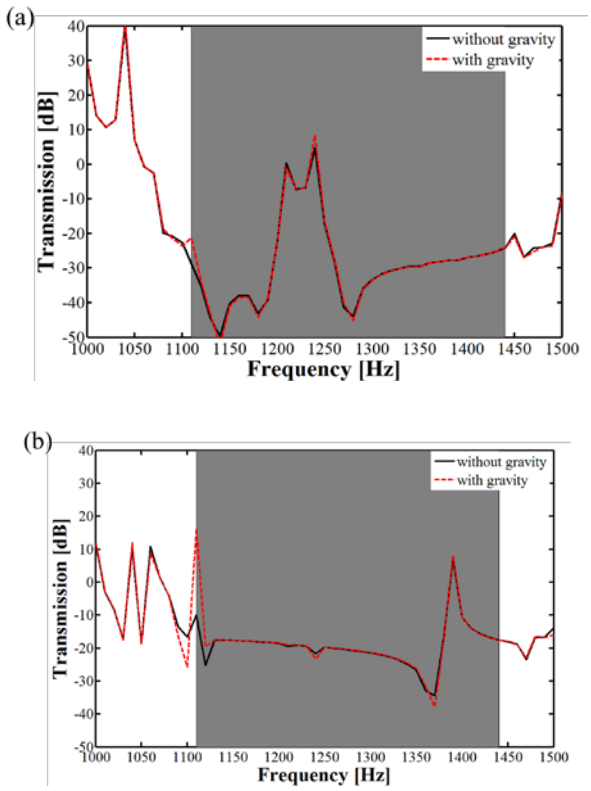

Fig. 6. Transmission diagrams along the (a) *x*- (or *y*-) and (b) *z*-directions with (red dashed lines) and without (black solid lines) the effect of gravity on the metaplate.

4.2. The effect of material damping

Material damping has an important effect on the isolation property of a metaplate since its presence naturally leads to spatial attenuation of waves and further changes in the transmission diagram. Therefore a lot of work has been done to study the effect of the material damping on the transmission diagram of metamaterials (D'Alessandro et al., 2016; Ardito et al., 2018; Lou et al., 2018).

Moreover, since it is known that the material properties of additive manufactured metaplates are highly dependent on specific printing parameters, it is difficult to calibrate the precise material damping for our structure. For this reason, here we introduce an isotropic damping factor (η) in the FEM model equal to 1% and 3% which are typical values for such kind of materials (Shahan and Fulcher, 2011)(John and Furukawa, 2009) (η=1% is verified by the experimental results in Section 5). In Fig. 7 the transmission diagrams along the *x*- (or *y*-) and *z*- directions are reported for different levels of material damping. As expected, the material damping increases the attenuation performance of the metaplate within band gaps and shifts in frequency the curve as already shown in (D'Alessandro et al., 2018). In the following, we consider the material damping η = 1% identified on experimental data reported in Section 5.

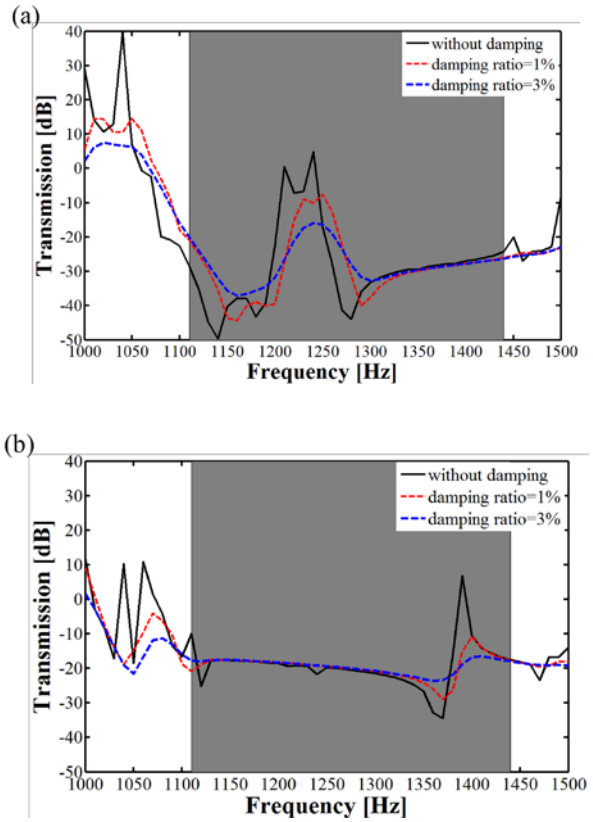

Fig. 7. Transmission diagrams along the (a) *x*- (or *y*-) and (b) *z*-directions computed by considering two material damping coefficients (red and blue dashed lines) and without considering the material damping (solid black lines).

4.3. The effect of central mass

In practical applications, the object to be isolated from vibrations is located in the central area of the metaplate. Therefore, it is necessary to study the effect of the central mass (mass of the object to be isolated from vibrations) on

the transmission diagram. By changing the thickness of the central mass in the numerical model, different masses of the isolated object are simulated. Fig. 8 shows the schematic view of the geometry of the metaplate with a central mass of 6 mm-thickness and a weight of about 9 g. The transmission diagrams with different thickness of central mass are shown in Fig. 9. From Fig. 9, one can observe that the frequency of the local modes (Figs. 4c-e) decreases with the increase of the thickness of the central mass such as the attenuation level in the *z*- axis transmission diagram.

We finally checked the effect of the gravity on the transmission diagram and we found very similar results to the ones reported in Section 4.1 (i.e. maximum *z*-axis displacement of 35.4 μm for the 6mm-thick central mass).

We can then conclude that it is possible to control the transmission spectrum inside the bandgap by changing the thickness of the central mass and the weight of the object to be isolated from vibration must be taken into account in the simulation process since it can modify the response of the metaplate.

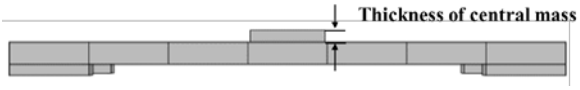

Fig. 8. Metaplate with the central mass of a 6mm thickness.

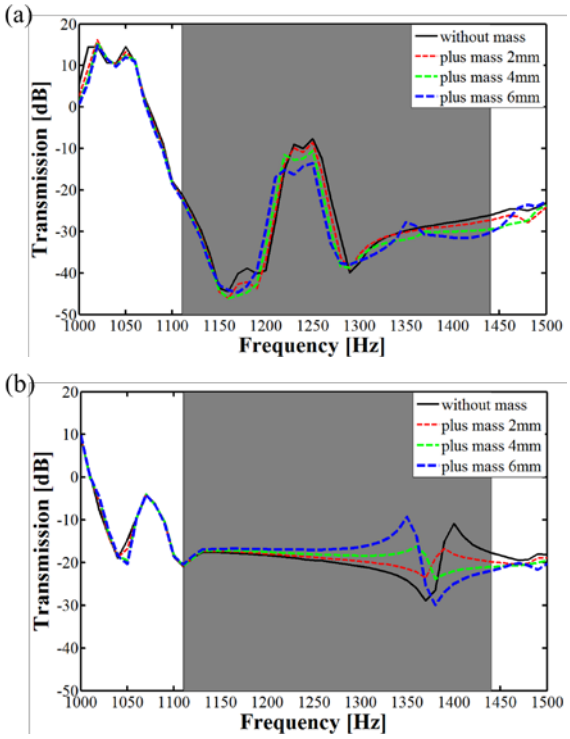

Fig. 9. Transmission diagram along the (a) *x*- (or *y*-) and (b) *z*-directions for different thicknesses of the central mass.

4.4. The effect of boundary conditions

To study the effect of different boundary conditions on the isolation property of the metaplate, the displacement excitation d_{in} is imposed in the middle of the plate and the average displacement response d_{out} is measured on the four anchor points (see Fig. 10). The transmission diagrams along the *x*- (or *y*-) and *z*- directions are shown in Figs 11a and b, respectively. A better attenuation level is found along the three directions and the peaks within the bandgap caused by the local modes disappear, thus improving a lot the isolation properties of the metaplate.

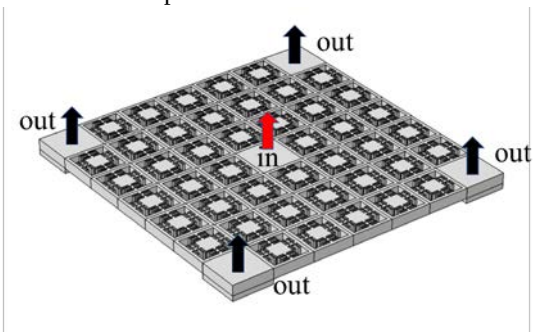

Fig. 10. Second configuration: input signal applied on the central area of the metaplate and output signal measured on the four anchor points.

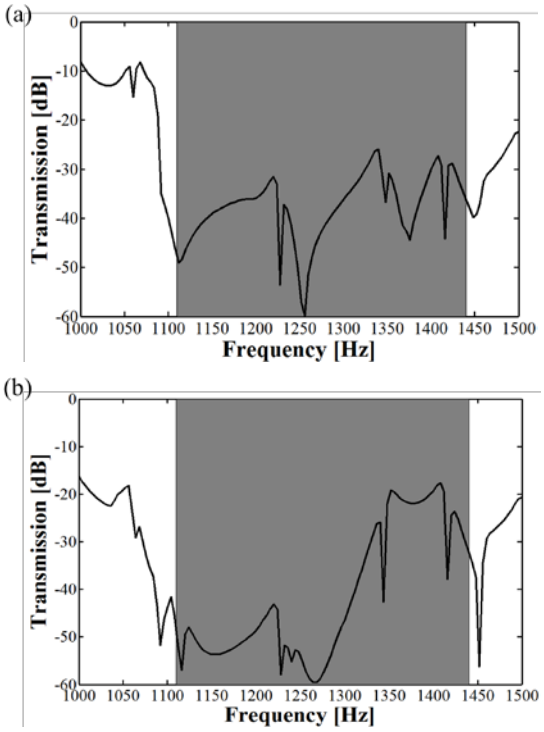

Fig. 11. Transmission diagram along (a) *x*- (or *y*-) and (b) *z*-directions computed by applying the boundary conditions shown in Fig. 9.

5. Experimental results and analysis

To experimentally demonstrate the existence of the bandgap, a prototype of the proposed metaplate has been fabricated through Selective Laser Sintering (SLS).

The excitation is applied by connecting the metaplate with a permanent magnet shaker LDS V455 with a frequency range from 5 Hz to 7.5 kHz and a power amplifier PA 100E (see Fig. 12a). Tests are performed with a white noise input of 20 kHz bandwidth applied along the *z*- direction. Four PCB Piezotronics 353C33 accelerometers, with a sensitivity of 100 mV/g and resonant frequency higher than 50 kHz, are placed at the center of faces (see Fig. 12b) to measure the output. The acquisition chain is then completed with 8-channel PCB sensor signal conditioner and two NI 9234 modules.

Data are then post-processed by MATLAB R2014b software in order to calculate the transmission diagram along the *z*- direction.

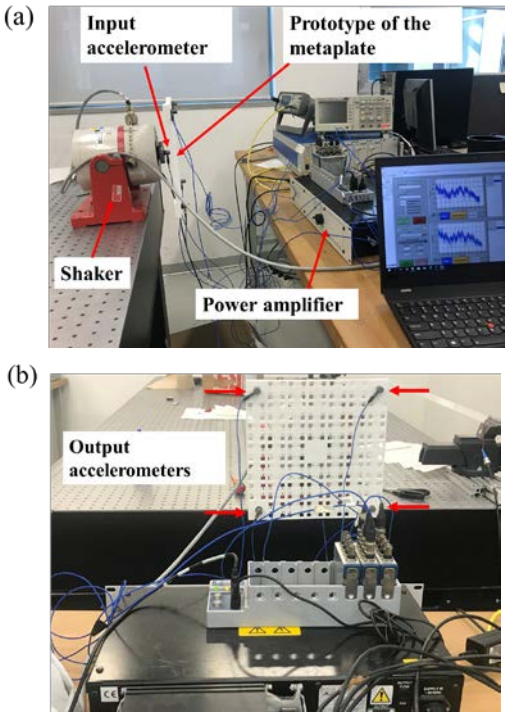

Fig. 12. (a) Side view and (b) front view of the experimental set-up.

The transmission diagrams (see Fig. 13a) measured by the four output accelerometers show vibration attenuations in the bandgap frequency range (reported as grey area in Fig. 13a) as expected. The transmission diagram computed through finite element analysis is then compared with the experimental results in Fig. 13b. The bandgap of the experimental transmission diagram of the 3D-printed metaplate well matches the theoretical prediction in terms of frequency range. Some discrepancies are instead evident if we compare the trends of the transmission diagrams. The difference can be caused by fabrication imperfections and by wrong estimation of the material parameters(i.e. material damping).

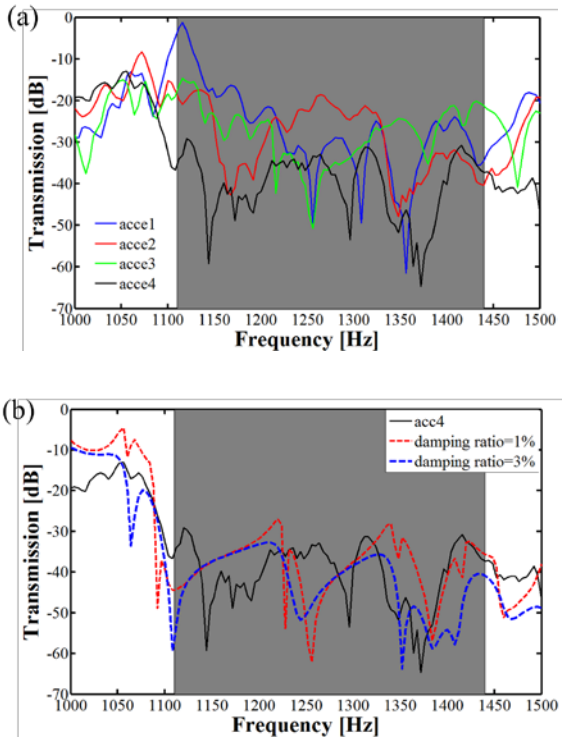

Fig. 13. (a) Experimental transmission diagrams along z- direction measured by the four output accelerometers (acce1-acce4, respectively). (b) Comparison between numerical results and experimental measurements.

6. Conclusion

A new metaplate with periodic ‘frame-springs-mass’ system is proposed for vibration isolation applications. A complete 3D bandgap is obtained around 1265 Hz, with a width of about 340 Hz.

Through the FEM calculation, we found that the gravity has almost no effect on the transmission diagram, the material damping causes the frequency shift in the transmission diagram, while the mass in the central area of the plate increases the attenuation level and moves the local modes in frequency. Moreover, we proved that the transmission depends on boundary conditions.

Experimental measurements agree well with the numerical results, thus proving the proposed idea that isolating low-frequency vibrations transmitted in metaplates is feasible and effective.

Acknowledgements

The authors thank Dr. Emanuele Riva and Prof. Francesco Braghin of the Mechanical Engineering Department of Politecnico di Milano for the precious support during the

experimental tests, Prosilas company for the accurate fabrication of the prototypes and China Scholarship Council (CSC) grant no.201806840034 for funding the author Z. Y. V.Z. and A.C. acknowledge the national project PRIN15 n. 2015LYYXA8.

References

Ardito, R., Alessandro, L.D., Corigliano, A., Braghin, F., 2018. Single-phase engineered metamaterials for wave filtering with optimal performances, in: EURONOISE 2018. pp. 7–10.

Ardito, R., Cremonesi, M., D'Alessandro, L., Frangi, A., 2016. Application of optimally-shaped phononic crystals to reduce anchor losses of MEMS resonators, in: IEEE International Ultrasonics Symposium, IUS. pp. 1–3. https://doi.org/10.1109/ULTSYM.2016.7728780

Badreddine Assouar, M., Oudich, M., 2012. Enlargement of a locally resonant sonic band gap by using double-sides stubbed phononic plates. Appl. Phys. Lett. 100, 123506. https://doi.org/10.1063/1.3696050

Bilal, O.R., Foehr, A., Daraio, C., 2017. Observation of trampoline phenomena in 3D-printed metamaterial plates. Extrem. Mech. Lett. 15, 103–107. https://doi.org/10.1016/j.eml.2017.06.004

Bilal, O.R., Hussein, M.I., 2013. Trampoline metamaterial: Local resonance enhancement by springboards. Appl. Phys. Lett. 103, 111901. https://doi.org/10.1063/1.4820796

Chen, J., Xia, Y., Han, X., Zhang, H., 2012. Lamb waves in phononic crystal slabs: Truncated plane parallels to the axis of periodicity. Ultrasonics 52, 920–924. https://doi.org/10.1016/j.ultras.2012.02.015

Chen, S., Wang, G., Song, Y., 2016. Low-frequency vibration isolation in sandwich plates by piezoelectric shunting arrays. Smart Mater. Struct. 25, 12504. https://doi.org/10.1088/0964-1726/25/12/125024

D'Alessandro, L., Belloni, E., Ardito, R., Braghin, F., Corigliano, A., 2017a. Mechanical low-frequency filter via modes separation in 3D periodic structures. Appl. Phys. Lett. 111, 231902. https://doi.org/10.1063/1.4995554

D'Alessandro, L., Belloni, E., Ardito, R., Corigliano, A., Braghin, F., 2016. Modeling and experimental verification of an ultra-wide bandgap in 3D phononic crystal. Appl. Phys. Lett. 109, 1–5. https://doi.org/10.1063/1.4971290

D'Alessandro, L., Belloni, E., D'Alo, G., Daniel, L., Ardito, R., Corigliano, A., Braghin, F., 2017b. Modelling and experimental verification of a single phase three-dimensional lightweight locally resonant elastic metamaterial with complete low frequency bandgap, in: 2017 11th International Congress on Engineered Material Platforms for Novel Wave Phenomena, Metamaterials 2017. pp. 70–72. https://doi.org/10.1109/MetaMaterials.2017.8107842

D'Alessandro, L., Zega, V., Ardito, R., Corigliano, A., 2018. 3D auxetic single material periodic structure with ultra-wide tunable bandgap. Sci. Rep. 8, 2262. https://doi.org/10.1038/s41598-018-19963-1

Dankowski, J., 1999. Low Frequency Shock and Vibration Isolation for Precision Engineering and Nanotechnology, in: Euspen Conference Proceedings. pp. 1–4.

Dian-Long, Y., Yao-Zong, L., Jing, Q., Hong-Gang, Z., Zhi-Ming, L., 2005. Experimental and Theoretical Research on the Vibrational Gaps in Two-Dimensional Three-Component Composite Thin Plates. Chinese Phys. Lett. 22, 1958–1960. https://doi.org/10.1088/0256-307x/22/8/038

Hedayatrasa, S., 2018. Design Optimisation and Validation of Phononic Crystal Plates for Manipulation of Elastodynamic Guided Waves. Springer Publishing, Berlin. https://doi.org/10.1007/978-3-319-72959-6

Hirsekorn, M., 2004. Small-size sonic crystals with strong attenuation bands in the audible frequency range. Appl. Phys. Lett. 84, 3364–3366. https://doi.org/10.1063/1.1723688

John, B., Furukawa, M., 2009. Enhanced Mechanical Properties of Polyamide 6 Fibers Coated with a Polyurethane Thin Film Baiju. Polym. Eng. Sci. 49, 1970–1978. https://doi.org/10.1002/pen

Khelif, A., Adibi, A., 2015. Phononic Crystals: Fundamentals and Applications. Springer Publishing, Berlin. https://doi.org/10.1007/978-1-4614-9393-8

Kushuwaha, M.S., 1993. Acoustic band structure of periodic elastic composites. Phys. Rev. Lett. 71, 2022–2025. https://doi.org/10.1103/PhysRevLett.71.2022

Li, S., Dou, Y., Chen, T., Xu, J., Li, B., Zhang, F., 2019. Designing a broad locally-resonant bandgap in a phononic crystals. Phys. Lett. Sect. A Gen. At. Solid State Phys. 383, 1371–1377. https://doi.org/10.1016/j.physleta.2019.01.061

Li, Y., Zhu, L., Chen, T., 2017. Plate-type elastic metamaterials for low-frequency broadband elastic wave attenuation. Ultrasonics 73, 34–42. https://doi.org/10.1016/j.ultras.2016.08.019

Liu, Z., Zhang, X., Mao, Y., Zhu, Y.Y., 2000. Locally Resonant Sonic Materials. Science. 289, 1734–1736. https://doi.org/10.1126/science.289.5485.1734

Lou, J., He, L., Yang, J., Kitipornchai, S., Wu, H., 2018. Wave propagation in viscoelastic phononic crystal rods with internal resonators. Appl. Acoust. 141, 382–392. https://doi.org/10.1016/j.apacoust.2018.07.029

Mei, J., Ma, G., Yang, M., Yang, Z., Wen, W., Sheng, P., 2012. Dark acoustic metamaterials as super absorbers for low-frequency sound. Nat. Commun. 3, 756–757. https://doi.org/10.1038/ncomms1758

Olsson, R.H., El-Kady, I.F., Su, M.F., Tuck, M.R., Fleming, J.G., 2008. Microfabricated VHF acoustic crystals and waveguides. Sensors Actuators, A Phys. 145–146, 87–93. https://doi.org/10.1016/j.sna.2007.10.081

Oudich, M., Li, Y., Assouar, B.M., Hou, Z., 2010. A sonic band gap based on the locally resonant phononic plates

with stubs. New J. Phys. 12, 083049. https://doi.org/10.1088/1367-2630/12/8/083049
Prosilas, Material parameters of Polyamide PA 2200. https://www.prosilas.com/en/polyamide/ (accessed 15 March 2019).
Ramsey, J., Wierschem, N., 2017. Passive control of the vibration of flooring systems using a gravity compensated non-linear energy sink, in: Proceedings of the 13th International Workshop on Advanced Smart Materials and Smart Structures Technology.
Reinke, C.M., Su, M.F., Olsson, R.H., El-Kady, I., 2011. Realization of optimal bandgaps in solid-solid, solid-air, and hybrid solid-air-solid phononic crystal slabs. Appl. Phys. Lett. 98, 2–5. https://doi.org/10.1063/1.3543848
Shahan, D., Fulcher, B., 2011. (), in: Proc. of 22nd Annual International Solid Freeform Fabrication Symposium-An Additive Manufacturing Conference (SFF 2011). pp. 719–732.
Wu, T.T., Huang, Z.G., Tsai, T.C., Wu, T.C., 2008. Evidence of complete band gap and resonances in a plate with periodic stubbed surface. Appl. Phys. Lett. 93, 111902. https://doi.org/10.1063/1.2970992
Xiao, Y., Wen, J., Wen, X., 2012. Sound transmission loss of metamaterial-based thin plates with multiple subwavelength arrays of attached resonators. J. Sound Vib. 331, 5408–5423. https://doi.org/10.1016/j.jsv.2012.07.016
Zhao, H.J., Guo, H.W., Gao, M.X., Liu, R.Q., Deng, Z.Q., 2016. Vibration band gaps in double-vibrator pillared phononic crystal plate. J. Appl. Phys. 119, 014903. https://doi.org/10.1063/1.4939484
Zhao, H.J., Guo, H.W., Li, B.Y., Deng, Z.Q., Liu, R.Q., 2015. Flexural vibration band gaps in a double-side phononic crystal plate. J. Appl. Phys. 118, 044906. https://doi.org/10.1063/1.4927627
Zhu, R., Huang, G.L., Huang, H.H., Sun, C.T., 2011. Experimental and numerical study of guided wave propagation in a thin metamaterial plate. Phys. Lett. Sect. A Gen. At. Solid State Phys. 375, 2863–2867. https://doi.org/10.1016/j.physleta.2011.06.006